reaction, the important result is that the complex becomes photochemically stable when involved in adducts with the aromatic crown ethers (except DB18C6). This behavior can be explained by an increase in the rate of radiationless decay of the Pt(bpy)$(NH_3)_2^{2+}$ excited states via the CT levels of the adduct and/or by a screening action performed by the host aromatic crown ethers on the guest platinum complex. The lack of quenching of the photoreaction for Pt(bpy)$(NH_3)^{2+}$·DB18C6 is consistent with the presence of the Pt(bpy)$(NH_3)_2^{2+}$ luminescence in this adduct and with the small size of the crown ring, which precludes the formation of a U-shape adduct as shown by CPK molecular models.

Electrochemistry. It is known that the +1 oxidation state of Pt is unstable[37] and that coordinated bpy ligand usually undergoes reversible or quasi-reversible one-electron reduction at a potential less negative than that corresponding to the reduction of free bpy.[38] The Pt$(bpy)_2^{2+}$ complex shows an irreversible reduction wave (assigned as metal centered) at −0.97 V and a partially reversible wave (assigned as ligand centered) at −1.51 V (AN solution, vs SCE).[39] Pt(bpy)$(NH_3)_2^{2+}$ shows an analogous behavior with an irreversible wave at −1.13 V and an almost reversible wave at −1.80 V. For the adduct with DB30C10 in AN solution (where there is an equilibrium with the free components) besides the two above-mentioned waves corresponding to the "free" Pt complex, two other waves were observed at −1.40 and −2.0 V. These waves can be assigned to the metal-centered and ligand-centered reductions of the complex in the adduct. The relative change in intensity of the waves on addition of an excess of host confirms this assignment. In CH_2Cl_2 solution only the adduct is present, and therefore only two reduction waves (concerning the metal and the ligand of the guest complex) are present.

Conclusions. The host–guest adducts obtained from Pt(bpy)$(NH_3)_2^{2+}$ and aromatic crown ethers are interesting and instructive systems for photochemical and photophysical investigations. The two molecular species are kept together by hydrogen bonds between the crown oxygen atoms and the NH_3 ligands of the complex (Figure 9). In addition, there is an electronic interaction between the bpy ligand of the complex and the aromatic rings of the crowns. Such an interaction causes strong changes in the extinction coefficients of the host- and guest-localized bands, the appearance of a CT absorption, the quenching (at room temperature) of the host and guest luminescence, the appearance of a new emission band characteristic of the adduct, and a change in the Pt(II)- and bpy-localized reduction processes. Furthermore, adduct formation protects the guest Pt(bpy)$(NH_3)_2^{2+}$ complex from giving the photoreaction observed for the free Pt(bpy)$(NH_3)_2^{2+}$ complex in CH_2Cl_2 solution. The perturbation effect on the properties of Pt(bpy)$(NH_3)_2^{2+}$ can be tuned by changing the size of the crown ring and the nature and substitution positions of the aromatic rings present in the crown.

Acknowledgment. We thank L. Minghetti and G. Gubellini for technical assistance. This work was supported by the Consiglio Nazionale delle Ricerche, the Ministero della Pubblica Istruzione, the Science and Engineering Research Council, and NATO (Grant No. 937/86).

Registry No. [Pt(bpy)$(NH_3)_2$]$(PF_6)_2$, 79953-62-1; [Pt(bpy)$(NH_3)_2$]$(PF_6)_2$·18C6, 79953-64-3; [Pt(bpy)$(NH_3)_2$]$(PF_6)_2$·DB18C6, 79953-65-4; [Pt(bpy)$(NH_3)_2$]$(PF_6)_2$·DB24C8, 79953-66-5; [Pt(bpy)$(NH_3)_2$]$(PF_6)_2$·DB30C10, 79953-63-2; [Pt(bpy)$(NH_3)_2$]$(PF_6)_2$·DB36C12, 79953-67-6; [Pt(bpy)$(NH_3)_2$]$(PF_6)_2$·BMP32C10, 121865-95-0; [Pt(bpy)$(NH_3)_2$]$(PF_6)_2$·BPP34C12, 121865-96-1; [Pt(bpy)$(NH_3)_2$]$(PF_6)_2$·DN30C10, 111121-42-7.

(37) Cotton, F. A.; Wilkinson, G. *Advanced Inorganic Chemistry*; John Wiley and Sons: New York, 1988.
(38) Vlcek, A. A. *Coord. Chem. Rev.* **1982**, *43*, 39.
(39) Chassot, L.; von Zelewsky, A. *Inorg. Chem.* **1987**, *26*, 2814.

Designed Synthesis of a Radical Cation Salt of Ni(tmp): Structural, Magnetic, and Charge-Transport Properties of Bis[(5,10,15,20-tetramethylporphyrinato)nickel(II)] Hexafluorophosphate

Timothy P. Newcomb, Martin R. Godfrey, Brian M. Hoffman,* and James A. Ibers*

Contribution from the Department of Chemistry and Materials Research Center, Northwestern University, Evanston, Illinois 60208. *Received December 19, 1988*

Abstract: Electrochemical oxidation of (5,10,15,20-tetramethylporphyrinato)nickel(II), Ni(tmp), in the presence of hexafluorophosphate ion affords the new molecular conductor $[Ni(tmp)]_2[PF_6]$, which is comprised of partially oxidized ($+^1/_2$) S_4-ruffled Ni(tmp) molecules stacked metal-over-metal. The PF_6^- anions lie within channels formed by adjacent porphyrin stacks on sites that minimize the porphyrin–hydrogen to –fluorine contacts. The choice of the PF_6^- anion, as being likely to produce an ordered crystal with this degree of partial oxidation, was prompted by an examination of the crystal structures of similar metallomacrocyclic conductors. ESR studies confirm the tmp ligand as the site of oxidation. Single-crystal room-temperature conductivity along the needle (crystallographic c) axis averages 75 Ω^{-1} cm^{-1}, somewhat lower than that observed for Ni(tmp)I and for most porphyrinic conductors containing larger porphyrins. The temperature dependence of the conductivity is metallic from room temperature to 205 K and decreases rapidly as the temperature is decreased further. Single-crystal X-ray diffraction measurements at 220 and 150 K demonstrate that this change in behavior does not result from a structural transition at 205 K. The compound crystallizes in space group D_{4h}^4–$P4/nnc$ of the tetragonal system with two formula units in a cell of dimensions a = 16.685 (1) Å and c = 6.994 (1) Å (volume = 1947 Å^3) at 220 K. The two Ni(tmp) molecules in the unit cell are separated by 3.497 (1) Å and are rotated with respect to one another by 34.7° (3)°. Full-matrix least-squares refinement of 76 variables gives a final value for the R index on F^2 of 0.127 for 1845 unique observations and a value of 0.045 for the R index on F for the 1243 observations having $F_o^2 > 3\sigma(F_o^2)$.

We have described a series of partially oxidized molecular conductors prepared by chemical oxidation of porphyrinic metallomacrocycles (M(L)) with molecular iodine.[1-6] A single structural motif has been retained throughout this series of ma-

0002-7863/89/1511-7078$01.50/0

terials, with metal-over-metal stacks of partially oxidized M(L) units surrounded by chains of I_3^- anions.[7] To date, iodine oxidation has never produced a macroscopically homogeneous and crystalline phase with a degree of partial oxidation other than $+^1/_3$. In addition, the chains of I_3^- anions are invariably disordered with respect to one another. This disorder is thought to affect the charge-transport properties. For example, we have speculated that the disorder of the iodine chains in Ni(pc)I may prevent a Peierls distortion and preserve high conductivity at very low temperatures in that compound.[6,8]

The present research has sought to vary of the degree of partial oxidation and band-filling in radical cation salts of M(tmp) (tmp = 5,10,15,20-tetramethylporphyrinato) while conserving the stacking structure of the metallomacrocycles and producing an ordered anion substructure. Metalloporphyrins, such as M(tmp), offer especially interesting systems for the study of band-filling effects. The two highest occupied molecular orbitals (HOMOs) of simple porphyrins are approximately degenerate and thus metalloporphyrin stacks should be two-band conductors. In contrast, macrocycles with larger conjugated ring systems (pc, tatbp, tbp)[2] and other well-known building blocks of molecular conductors (e.g., TMTSF, ET, $Ni(dmit)_2$, etc.)[8,9] all have nondegenerate HOMOs and can only form a single conduction band.

The strategy employed here involves the careful choice of anion upon consideration of analogous electrocrystallizations of benzoporphyrins, such as phthalocyanine. It has enabled us to prepare bis[(5,10,15,20-tetramethylporphyrinato)nickel(II)] hexafluorophosphate, $[Ni(tmp)]_2[PF_6]$, a compound with $+^1/_2$ degree of partial oxidation and three-dimensionally ordered anions. After discussing the considerations involved in the choice of the PF_6^- anion, we report the structural, magnetic, and charge-transport properties of this compound.

Synthetic Strategy

Our approach to the preparation of $[Ni(tmp)]_2[PF_6]$ is based on an examination of the crystal structure of Ni(tmp)I.[1] This structure exhibits two distinct crystallographic sites in which anions reside. These sites alternate along channels formed by the Ni(tmp) stacks. In the Ni(tmp)I structure, the iodine atoms lie in chains along a 4-fold axis coincident with $^1/_4$, $^1/_4$, z. The sites at $z = {}^1/_4$ and $z = {}^3/_4$ correspond to special positions 2a and 2b, both of which have 42 (D_4) symmetry. These sites lie between constrictions in the channels caused by steric interactions of surrounding Ni(tmp) molecules and are the center of relatively large cavities in these channels. The two sites do not have identical environments, and if an anion were to reside exclusively in one site at 100% occupancy an ordered phase with a $+^1/_2$ degree of partial oxidation would be produced.

The key to achieving exclusive occupancy is to select anions that are of the proper size to occupy a specific site in such a crystal structure. This choice is guided by other recent electrocrystallization studies. A degree of partial oxidation of $+^1/_2$ has been reported for Ni(pc) in $[Ni(pc)]_2[SbF_6]$ and $[Ni(pc)]_2[AsF_6]$.[10a] The anions of the SbF_6^- salt form chains in the channels between the Ni(pc) stacks occupying only one possible site and are consequently ordered. However, these anions are so large that they cause a slight distortion of the Ni(pc) stacks. Because of its smaller size the AsF_6^- anion does not distort the structure of the metallomacrocycle stacks, but adjacent chains of anions are disordered with respect to one another in the same way as the I_3^- anions of Ni(pc)I. The ClO_4^- anion is so small that in the compound $[Ni(pc)][ClO_4]_y$, $y = 0.39$–0.47, the anions not only disorder rotationally and translationally but produce crystals of varying stoichiometry.[10b] Although the issue of design was not addressed in any of these studies, they provide a foundation for a rational approach.

These examples demonstrate that anion size can determine the structure and stoichiometry of the $[M(L)]_x[A]$ class of molecular metals. The channels formed in Ni(tmp)I are more constricted than the channels found in $[Ni(pc)]_x[A]$ conductors. Therefore, we reasoned that anions of a size intermediate between AsF_6^- and ClO_4^- might be of ideal size to occupy either site 2a or site 2b in the Ni(tmp) channels. The PF_6^- anion was the obvious first choice to fill these requirements in the preparation of Ni(tmp) radical cation salts. It is important to note that the same considerations have enabled us to choose an anion that would lead to an ordered salt of a partially oxidized benzoporphyrin; we report elsewhere the preparation and properties of $[Cu(tatbp)]_3[ReO_4]_2 \cdot C_{10}H_7Cl$.[11]

Experimental Section

Preparation of $[Ni(tmp)]_2[PF_6]$. Ni(tmp) was prepared as described previously.[12] Single crystals of $[Ni(tmp)]_2[PF_6]$ were grown at the anode of an electrolytic cell that consisted of two compartments separated by a medium porosity frit. The anode compartment was filled with a 1,1,2-trichloroethane solution that was 10^{-3} M in Ni(tmp) and 10^{-2} M in $[N(n\text{-}Bu)_4][PF_6]$. The cathode compartment was filled with a 1,1,2-trichloroethane solution that was 10^{-2} M in $[N(n\text{-}Bu)_4][PF_6]$. Platinum electrodes were immersed in both compartments, and a constant current of 2 μA was passed through the cell for 1 week. Needlelike crystals of $[Ni(tmp)]_2[PF_6]$, octagonal in cross section, were harvested from the anode surface.

The reduction of the $N(n\text{-}Bu)_4^+$ cation in trichloroethane results in the formation of Cl^- anions,[13] which may migrate into the anode compartment. Random crystals were specifically examined for chlorine contamination with the use of an EDAX-equipped scanning electron microscope. No chlorine was detected. Semiquantitative EDAX analysis determined the Ni/P atom ratio to be approximately 2/1. Elemental analyses were carried out by Galbraith Laboratories, Inc., Knoxville, TN, and are consistent with the formula $[Ni(tmp)]_2[PF_6]$. Anal. Calcd for $C_{48}H_{40}F_6N_8Ni_2P$: C, 58.16; H, 4.07; N, 11.30. Found: C, 58.01; H, 4.12; N, 11.24.

X-ray Diffraction Study of $[Ni(tmp)]_2[PF_6]$. From Weissenberg photographs, crystals of $[Ni(tmp)]_2[PF_6]$ were assigned to Laue group 4/*mmm* of the tetragonal system. The systematic absences ($hk0$, $h + k$ odd; $0kl$, $k + l$ odd; hhl, l odd) are consistent only with space group D_{4h}^4–$P4/nnc$. These photographs are superimposable on photographs of Ni(tmp)I. The structure of Ni(tmp)I was determined at 114 K, a temperature higher than an observed conductivity transition from metallic

(1) Pace, L. J.; Martinsen, J.; Ulman, A.; Hoffman, B. M.; Ibers, J. A. *J. Am. Chem. Soc.* **1983**, *105*, 2612–2620.
(2) Hoffman, B. M.; Ibers, J. A. *Acc. Chem. Res.* **1983**, *16*, 15–21.
(3) (a) Ogawa, M. Y.; Hoffman, B. M.; Lee, S.; Yadkowsky, M.; Halperin, W. P. *Phys. Rev. Lett.* **1986**, *57*, 1177–1180. (b) Martinsen, J.; Stanton, J. L.; Greene, R. L.; Tanaka, J.; Hoffman, B. M.; Ibers, J. A. *J. Am. Chem. Soc.* **1985**, *107*, 6915–6920.
(4) Martinsen, J.; Pace, L. J.; Phillips, T. E. Hoffman, B. M.; Ibers, J. A. *J. Am. Chem. Soc.* **1982**, *104*, 83–91.
(5) Phillips, T. E.; Scaringe, R. P.; Hoffman, B. M.; Ibers, J. A. *J. Am. Chem. Soc.* **1980**, *102*, 3435–3444.
(6) Schramm, C. J.; Scaringe, R. P.; Stojakovic, D. R.; Hoffman, B. M.; Ibers, J. A.; Marks, T. J. *J. Am. Chem. Soc.* **1980**, *102*, 6702–6713.
(7) Other structural types have been prepared with M(pc) systems of higher coordination number. For example see: (a) Wynne, K. J. *Inorg. Chem.* **1985**, *24*, 1339–43. (b) Hanack, M. *Mol. Cryst. Liq. Cryst.* **1988**, *160*, 133–7. (c) Mossoyan-Deneux, M.; Benlian, D.; Baldy, A.; Pierrot, M. *Mol. Cryst. Liq. Cryst.* **1988**, *156*, 247–56. (d) Mossoyan-Deneux, M.; Benlian, D.; Pierrot, M.; Fournel, A.; Sorbier, J. P. *Inorg. Chem.* **1985**, *24*, 1878–82. (e) Pietro, W. J.; Marks, T. J.; Ratner, M. A. *J. Am. Chem. Soc.* **1985**, *107*, 5387–5391.
(8) Abbreviations used: tmp, 5,10,15,20-tetramethylporphyrinato; tbp, tetrabenzoporphyrinato; tatbp, triazatetrabenzoporphyrinato; omtbp, 1,4,5,8,9,12,13,16-octamethyltetrabenzoporphyrinato; pc, phthalocyaninato; oep, 2,3,7,8,12,13,17,18-octaethylporphyrinato; TMTSF, tetramethyltetraselenafulvalene; ET, bis(ethylenedithiolo)tetrathiafulvalene; *n*-Bu, *n*-butyl; dmit, 1,3-dithiol-2-thione-4,5-dithiolato.
(9) (a) Williams, J. M.; Beno, M. A.; Wang, H. H.; Leung, P. C. W.; Emge, T. J.; Geiser, U.; Carlson, K. D. *Acc. Chem. Res.* **1985**, *18*, 261–267. (b) Torrance, J. B. *Acc. Chem. Res.* **1979**, *12*, 79–86. (c) Bousseau, M.; Valade, L.; Legros, J.; Cassoux, P.; Garbauskas, M.; Interrante, L. V. *J. Am. Chem. Soc.* **1986**, *108*, 1908–1916. (d) Kato, R.; Kobayashi, H.; Kobayashi, A.; Sasaki, Y. *Chem. Lett.* **1985**, 131–134. (e) Underhill, A. E.; Tonge, J. S.; Clemenson, P. I.; Wang, H. H.; Williams, J. M. *Mol. Cryst. Liq. Cryst.* **1985**, *125*, 439–446.
(10) (a) Yakushi, K.; Sakuda, M.; Hamada, I.; Kuroda, H.; Kawamoto, A.; Tanaka, J.; Sugano, T.; Kinoshita, M. *Synth. Met.* **1987**, *19*, 769–774. (b) Almeida, M.; Kanatzidis, M. G.; Tonge, L. M.; Marks, T. J.; Marcy, H. O.; McCarthy, W. J.; Kannewurf, C. R. *Solid State Commun.* **1987**, *63*, 457–461.
(11) Godfrey, M. R.; Liou, K. K.; Newcomb, T. P.; Halperin, W. P.; Hoffman, B. M.; Ibers, J. A. *Synth. Met.* **1989**, *29*, F51–F58.
(12) (a) Ulman, A.; Gallucci, J.; Fisher, D.; Ibers, J. A. *J. Am. Chem. Soc.* **1980**, *102*, 6852–6854. (b) Ulman, A.; Fisher, D.; Ibers, J. A. *J. Heterocycl. Chem.* **1982**, *19*, 409–413.
(13) Anzai, H.; Tokumoto, M.; Saito, G. *Mol. Cryst. Liq. Cryst.* **1985**, *125*, 385–392.

Table I. Crystal Data and Experimental Details for $[Ni(tmp)]_2[PF_6]$

compd	bis(5,10,15,20-tetramethylporphyrinato)-nickel(II)] hexafluorophosphate
formula	$C_{48}H_{40}F_6N_8Ni_2P$
formual wt, amu	991.29
cell	
a, Å	16.685 (1)
c, Å	6.994 (1)
V, Å^2	1947
Z	2
temp,[a] K	220
d_{calc}, g/cm^3	1.690
d_{obs}, g/cm^3 [b]	1.70 (4)
space group	D_{4h}^4–$P4/nnc$
crystal shape	needles of octagonal cross section bounded by faces of the forms {100}, {110}, {001} with separations of 0.132, 0.135, 0.128, 0.128, 0.733 mm, respectively
crystal vol, mm^3	0.0126
radiation	Mo Kα (λ(Mo Kα_1) = 0.7093 Å)
μ, cm^{-1} [c]	10.9
transmission factors	0.87–0.89
take-off angle, deg	2.5
receiving aperture	2.5-mm vertical × 2.0-mm horizontal; 20 cm from crystal
scan speed, deg/min	4($2.5 \le \theta \le 26$), 2($26 \le \theta \le 33$); for reflections with $I < 3\sigma(I)$, rescans were forced to achieve $I > 3\sigma(I)$, up to 100 s total scan time
background counts	$^1/_4$ scan range on each side of reflections
scan method	θ–2θ
scan range, θ	–0.35 below Kα_1 to 0.35 above Kα_2
std reflections	six std reflections, scanned every 3 h of X-ray exposure time
collection limits	$2.5° \le \theta \le 33.0°$; $0.061 \le \lambda^{-1} \sin\theta \le 0.768$ Å^{-1}
data collected	$h, k, l \ge 0$
p factor	0.04
no. of data collected	4121
no. of unique data (including $F_o^2 < 0$)	1845
no. of unique data ($F_o^2 \ge 3\sigma(F_o^2)$)	1243
no. of variables	76
R on F_o^2	0.127
R_w on F_o^2	0.120
R on F_o, $F_o^2 > 3\sigma(F_o^2)$	0.045
R_w on F_o, $F_o^2 > 3\sigma(F_o^2$e)	0.058
error in obsd unit wt	1.42e^2

[a] The low-temperature system is from a design by J.-J. Bonnet and S. Askenazy, Sotorem, Z. I. de Vic, 31320 Castanet-Tolosan, France. [b] Flotation in CH_2Br_2/CCl_4 at room temperature. [c] The analytical absorption correction was performed with use of the Northwestern absorption program AGNOST. See: de Meulenaer, J.; Tompa, H.; *Acta Crystallogr.* **1965**, *19*, 1014–1018.

to activated behavior.[1] The conductivity behavior of $[Ni(tmp)]_2[PF_6]$ also undergoes this type of transition, but at 205 K (vide infra). The structure of $[Ni(tmp)]_2[PF_6]$ was determined at 220 K, 15 deg above the conductivity transition, in order to establish a reliable comparison with Ni(tmp)I. The cell constants of a = 16.685 (1) Å and c = 6.994 (1) Å at 220 K were determined by a least-squares refinement of the setting angles of 25 reflections that had been centered on an Enraf-Nonius CAD4 diffractometer. The density of 1.70 (4) g/cm^3 observed at room temperature compares well to that of 1.69 g/cm^3 calculated for two formula units in the 220 K cell. Intensity data were collected at 220 K by the θ–2θ technique and were processed by methods standard in this laboratory.[14] A total of 4121 reflections were collected, of which 1845 are unique and of these 1243 have $F_o^2 > 3\sigma(F_o^2)$. Crystal data and experimental details are summarized in Table I.

A Patterson map indicated that the position of the phosphorus atom is displaced 0, $^1/_2$, $^1/_4$ from the nickel atom. This constraint and the presence of two formula units per cell limit the possible special position for the nickel atoms in $P4/nnc$ (unit cell origin at $\bar{1}$) to either 4d, with $\bar{4}$ symmetry, or 2a or 2b, both with 42 symmetry. In Ni(tmp)I, the orientation of the porphyrin ring was determined by examination of iodine-to-ring atom vectors; the nickel atom position is on the $\bar{4}$ site. A check of phosphorus-to-ring vectors revealed, not surprisingly, the same trend; we thus placed the nickel atom in the 4d position.

Table II. Positional and Equivalent Isotropic Thermal Parameters for $[Ni(tmp)]_2[PF_6]$

atom	x	y	z	B
Ni	$^3/_4$	$^1/_4$	$^1/_2$	1.489 (7)
P	$^3/_4$	$^3/_4$	$^1/_4$	3.48 (4)
F(1)	$^3/_4$	$^3/_4$	0.0416 (14)	23.4 (4)
F(2)	0.81461 (14)	0.81461	$^1/_4$	14.0 (2)
N	0.852480 (95)	0.196249 (97)	0.515 21 (22)	1.74 (3)
C(1)	0.927 33 (12)	0.229 80 (13)	0.508 38 (29)	1.97 (4)
C(2)	0.987 94 (13)	0.171 82 (14)	0.553 77 (35)	2.59 (5)
C(3)	0.950 01 (13)	0.101 36 (13)	0.585 07 (34)	2.57 (5)
C(4)	0.865 95 (12)	0.115 54 (12)	0.554 45 (30)	1.99 (4)
C(5)	0.809 27 (13)	0.055 39 (11)	0.541 08 (29)	2.09 (4)
C(6)	0.834 65 (15)	–0.031 12 (13)	0.563 71 (37)	2.89 (5)
H(1)C(2)	0.045	0.182	0.562	3.6
H(1)C(3)	0.974	0.051	0.622	3.6
H(1)C(6)	0.793	–0.060	0.631	3.9
H(2)C(6)	0.842	–0.055	0.443	3.9
H(3)C(6)	0.883	–0.034	0.635	3.9

Initial refinements were carried out on F_o with the 1243 unique reflections having $F_o^2 > 3\sigma(F_o^2)$. All non-hydrogen atom positions were determined from subsequent electron density maps. The data were then corrected for absorption, and equivalent reflections (hkl, khl) were averaged. Least-squares refinement on F_o with isotropic thermal parameters of all non-hydrogen atoms led to values of R and R_w of 0.10 and 0.15, respectively. When anisotropic thermal parameters were used, R and R_w decreased to 0.056 and 0.082, respectively. All hydrogen atoms were located on a difference electron density map and their positions idealized (C–H = 0.95 Å) and not varied. Each hydrogen atom was assigned a thermal parameter 1 Å^2 greater than the equivalent isotropic thermal parameter of the carbon atom to which it is bonded. The final refinement was carried out on F_o^2 and involved 76 variables and all 1845 unique data (including $F_o^2 < 0$). This refinement converged to the agreement indexes given in Table I. Final positional and thermal parameters are given in Table II. Table III presents the anisotropic thermal parameters.[15] Table IV[15] provides a listing of $10|F_o|$ versus $10|F_c|$.

We determined the structure of $[Ni(tmp)]_2[PF_6]$ at 150 K and found it to be identical with that determined at 220 K. Thus, the conductivity transition does not correspond to a change in structure. Unfortunately, the crystal used for data collection at 220 K was lost. A second, much smaller crystal was examined at 150 K. The unit cell size undergoes a minor contraction (a = 16.583 (8) Å, c = 6.952 (3) Å). In the final refinement, the following R indexes were obtained: $R(F^2)$, 0.131, 1275 observations; $R(F)$, 0.069, 473 observations. There are no significant differences in positional parameters determined at 150 and 220 K. We report the latter here because they are more precise.

Electron-Spin Resonance Measurements. Powder and single-crystal electron-spin resonance spectra were obtained on a modified Varian E-4 X-band spectrometer with 100-kHz field modulation as described previously.[5] A single crystal of $[Ni(tmp)]_2[PF_6]$ was mounted on a quartz rod that was attached to a goniometer and placed in the resonance cavity of the spectrometer. The crystal was oriented such that the needle (c) axis could be positioned parallel or perpendicular to the applied field and rotated through intermediate angles. Rotation angles were measured to a precision of ±1.0°.

Magnetic Susceptibility Measurements. Static magnetic susceptibility measurements were taken with an S.H.E. VTS-50 SQUID susceptometer. The sample holder was made of high-purity Spectrosil quartz (Thermal American Fused Quartz Co., Montville, NJ) and its background magnetic contribution was measured over the full temperature range just prior to measuring the sample. The sample magnetism was determined, at a field strength of 5 kG, from the average of 10 measurements made at each temperature. The sample weight was 28 mg.

Single-Crystal Electrical Conductivity Measurements. The electrical conductivity along the needle (c) axis of single crystals of $[Ni(tmp)]_2[PF_6]$ was measured with a four-probe ac (27-Hz) phase-locked technique described previously.[16] The temperature was controlled with a nitrogen gas flow system and monitored to a precision of ±1.0 K with a copper–constantan thermocouple located within the sample holder. The rate of cooling varied between 0.5 and 0.1 deg/min. A given crystal was mounted on four thin (8-μm) graphite fibers that had been attached to four aluminum wires in an integrated circuit can.[16] All electrical contacts

(14) Corfield, P. W. R.; Doedens, R. J.; Ibers, J. A. *Inorg. Chem.* **1967**, *6*, 197–204.

(15) Supplementary material.

(16) Phillips, T. E.; Anderson, J. R.; Schramm, C. J.; Hoffman, B. M. *Rev. Sci. Instrum.* **1979**, *50*, 263–265.

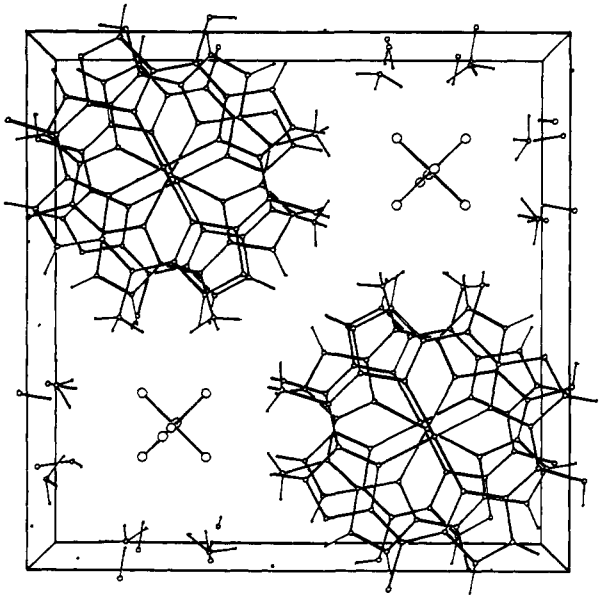

Figure 1. $[Ni(tmp)]_2[PF_6]$ structure as viewed along the [001] direction. Hydrogen atoms have been drawn arbitrarily small.

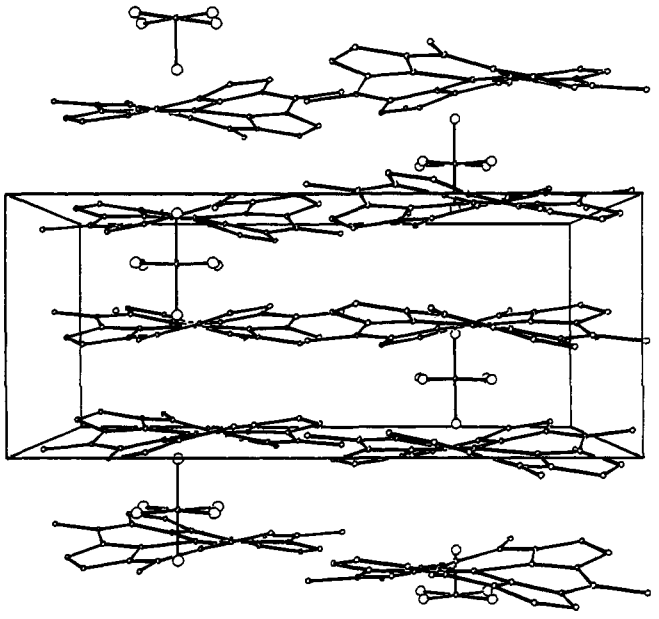

Figure 2. $[Ni(tmp)]_2[PF_6]$ structure as viewed along the [010] direction. Hydrogen atoms have been omitted for clarity.

were made with a conductive silver paint (Du Pont, conductor composition 4929). A sampling current of 10 μA was passed through the two outer contacts, and the voltage drop across the inner contacts was measured. The conductivity, $\sigma_\parallel$ (Ω^{-1} cm^{-1}), was calculated from the relation $\sigma_\parallel = L/(R_\parallel A)$ where L is the separation between the two inner contacts of the four probes, A is the cross-sectional area of the crystal, and $R_\parallel$ is the resistance. The dimensional parameters, L and A, varied within the ranges 0.1–0.3 mm and 1×10^{-6}–6.4×10^{-3} mm^2, respectively. The uncertainties in the measurements of sample dimensions are estimated to cause an uncertainty in the absolute conductivity of $\Delta\sigma/\sigma = \pm 0.2$. These needle-shaped crystals are too thin to enable the measurement of conductivity perpendicular to the needle axis.

Results and Discussion

Description of the Structure. The unit cell constants of $[Ni(tmp)]_2[PF_6]$ are essentially the same as those for Ni(tmp)I,[1] and both crystallize in space group $P4/nnc$. Both compounds are composed of columns of S_4-ruffled Ni(tmp) cations, surrounded by chains of anions. The Ni(tmp) columns in $[Ni(tmp)]_2[PF_6]$ are isostructural with those of Ni(tmp)I, and the two crystal structures differ only in the arrangement of the anions. Figure 1 shows the stacking of Ni(tmp) cations as viewed along the [001] direction. These cations have crystallographically imposed $\bar{4}$ symmetry and stack metal-over-metal with their mean planes orthogonal to the c axis. The anion chains lie in the channels formed by the Ni(tmp) columns. This relationship is depicted in Figure 2.

Ni(tmp) Cation. A drawing of the Ni(tmp) cation with labeling scheme is shown in Figure 3. Table V summarizes the intramolecular bond distances and angles for $[Ni(tmp)]_2[PF_6]$ at 220 K. The best weighted least-squares planes are given in Table VI. The mean molecular plane is constrained by symmetry to be at

Table V. Bond Distances and Angles for $[Ni(tmp)]_2[PF_6]$ at 220 K[a]

bond	type[b]	distance	av[c]
Ni–N	M–N	1.933 (2)	
N–C(1)	N–C_a	1.371 (3)	1.383 (16)
N–C(4)		1.394 (3)	
C(1)–C(2)	C_a–C_b	1.439 (3)	1.439 (3)
C(3)–C(4)		1.439 (3)	
C(2)–C(3)	C_b–C_b	1.354 (3)	
C(1)–C(5)	C_a–C_b	1.399 (3)	1.390 (10)
C(4)–C(5)		1.380 (3)	
C(5)–C(6)	C_m–C_t	1.509 (3)	
P–F(1)		1.455 (10)	
P–F(2)		1.524 (2)	

atoms	type	angle	av
N–Ni–N	N–M–N′	90.17 (1)	
Ni–N–C(1)	M–N–C_a	127.8 (1)	127.4 (6)
Ni–N–C(4)		127.0 (1)	
C(1)–N–C(4)	C_a–N–C_a	105.0 (1)	
N–C(1)–C(2)	N–C_a–C_b	110.8 (2)	110.5 (4)
N–C(4)–C(3)		110.2 (2)	
N–C(1)–C(5)	N–C_a–C_m	125.9 (2)	125.7 (3)
N–C(4)–C(5)		125.5 (2)	
C(1)–C(2)–C(3)	C_a–C_b	107.1 (2)	107.0 (2)
C(2)–C(3)–C(4)		106.8 (2)	
C(2)–C(1)–C(5)	C_b–C_a–C_m	123.2 (2)	123.5 (3)
C(3)–C(4)–C(5)		123.8 (2)	
C(1)–C(5)–C(4)	C_a–C_m–C_a	120.8 (2)	
C(1)–C(5)–C(6)	C_a–C_m–C_t	119.7 (2)	119.5 (3)
C(4)–C(5)–C(6)		119.3 (2)	

[a] Rotation angle between intrastack Ni(tmp) molecules: 34.7 (3)°. [b] The notation is that of Hoard (Hoard, J. L. *Science* (*Washington D. C.*) **1971**, *174*, 1295–1302): C_t is the methyl group on the methine carbon atom. [c] Average values are weighted. The error is taken to be the larger of the unweighted estimated standard deviation of a single observation as estimated from the inverse matrix or from the values averaged.

Table VI. Least-Squares Planes in $[Ni(tmp)]_2[PF_6]$

atom	plane 1[a]	plane 2, pyrrole ring
Ni	0	
N	0.106 (2)[b]	−0.015 (2)[b]
C(1)	0.059 (2)	0.016 (2)
C(2)	0.376 (3)	−0.002 (2)
C(3)	0.595 (2)	−0.017 (2)
C(4)	0.381 (2)	−0.024 (2)
C(5)	0.287 (2)	0.251
C(6)	0.446	0.440
av dev	0.301	0.015

	plane equation: $Ax + By + Cz = D$			
plane	A	B	C	D
1	0	0	6.994	3.497
2[c]	3.565	1.393	6.807	6.672

[a] Plane is defined by the porphyrin 24-atom core. [b] Standard deviations are given for those atoms used in the definition of the plane. [c] The dihedral angle between plane 1 and plane 2 is 13.3°.

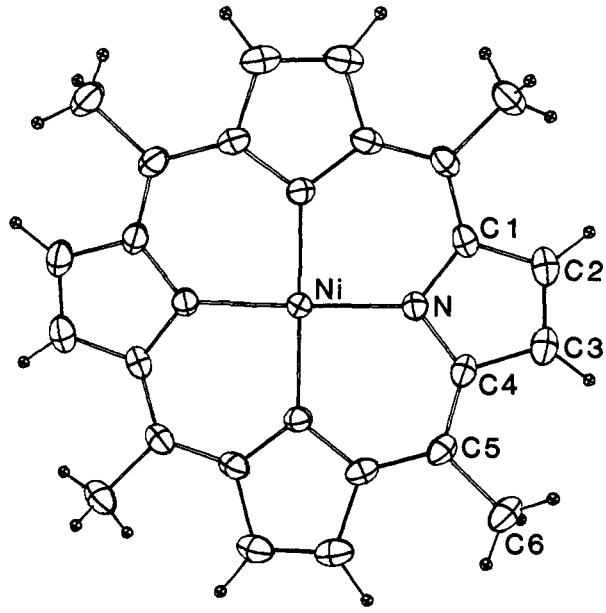

Figure 3. Drawtng of the Ni(tmp) cation with labeling scheme. Hydrogen atoms have been drawn arbitrarily small.

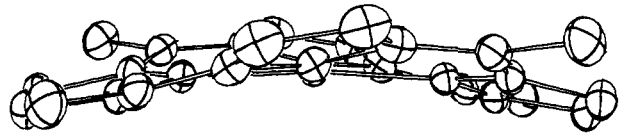

Figure 4. View of the Ni(tmp) cation in $[Ni(tmp)]_2[PF_6]$ at 220 K as viewed down a Ni–N bond. Hydrogen atoms have been omitted.

$z = {}^1/_2$. However, the cation (symmetry $\bar{4}$) is nonplanar. Each pyrrole ring is tilted $\sim 13°$ from the mean plane to produce the saddle shape depicted in Figure 4. The Ni(tmp) bond distances and angles found in $[Ni(tmp)]_2[PF_6]$ are indistinguishable from those found for Ni(tmp) in Ni(tmp)I.

PF_6^- Anion. The phosphorus atoms are located on sites of imposed 42 symmetry (site 2b). The two crystallographically unique fluorine atoms (axial F(1) and equatorial F(2)) form a distorted octahedron about the phosphorus atom. Though the P–F distances are not unexpected,[17] the axial bond lengths are shorter than the equatorial bond lengths, and the octahedron is constricted along the 4-fold axis. In contrast to the disordered I_3^- anion chains in Ni(tmp)I,[1] the chains of PF_6^- anions appear to be ordered in $[Ni(tmp)]_2[PF_6]$. The high thermal parameters of the F atoms may indicate some measure of static disorder. The location of the phosphorus atoms, and hence the PF_6^- anions, in site 2b as opposed to site 2a (also of 42 symmetry) may be rationalized in terms of the hydrogen-to-fluorine contacts within the channels. The two sites, 2a and 2b, do not possess identical environments. The ${}^1/_4, {}^1/_4, {}^1/_4$ (site 2a) position is more constrained than the ${}^1/_4, {}^1/_4, {}^3/_4$ (site 2b) position. A PF_6^- anion located at ${}^1/_4, {}^1/_4, {}^1/_4$ would experience H–F(2) (equatorial F) contacts of 2.2–3.4 Å. The corresponding contacts for the anion at ${}^1/_4, {}^1/_4, {}^3/_4$ are significantly longer, 2.6–3.9 Å. This situation is also true, though not as dramatic, for the H–F(1) (axial F) contacts; the ${}^1/_4, {}^1/_4, {}^3/_4$ position offers ~0.1 Å more room than the ${}^1/_4, {}^1/_4, {}^1/_4$ position. No peaks were observed at ${}^1/_4, {}^1/_4, {}^1/_4$ in a difference electron density map.

Electron-Spin Resonance. Powdered samples of $[Ni(tmp)]_2[PF_6]$ have a measured g value near that of a free electron, g_{avg} = 2.005 (1). This value confirms the tmp ring as the site of oxidation. The angle dependence of the g tensor for a single crystal is axially symmetric and may be described by

$$g(\theta) = [g_\parallel^2 \cos^2\theta + g_\perp^2 \sin^2\theta]^{1/2} \quad (1)$$

where θ is the angle between the applied magnetic field and the crystal c axis. A fit of the experimental data for $[Ni(tmp)]_2[PF_6]$ to eq 1 yields $g_\perp > g_\parallel \sim g_e$ ($\Delta g = g_\perp - g_\parallel = 0.001$) as expected for a π-cation radical.[18] This was not the case for Ni(tmp)I where $g_\parallel > g_\perp \sim g_e$ indicated a small amount of back-charge transfer from the I_3^- anion to the Ni(tmp) ring.[1] No change in the g value of $[Ni(tmp)]_2[PF_6]$ was observed upon cooling a sample to 77 K, consistent with the behavior of previously reported[1,6] one-dimensional nickel macrocyclic conductors.

The ESR line shape for $[Ni(tmp)]_2[PF_6]$ single crystals is approximately Lorentzian from room temperature to 77 K. The room-temperature peak-to-peak derivative line width, Γ, is axially symmetric with an angular dependence of

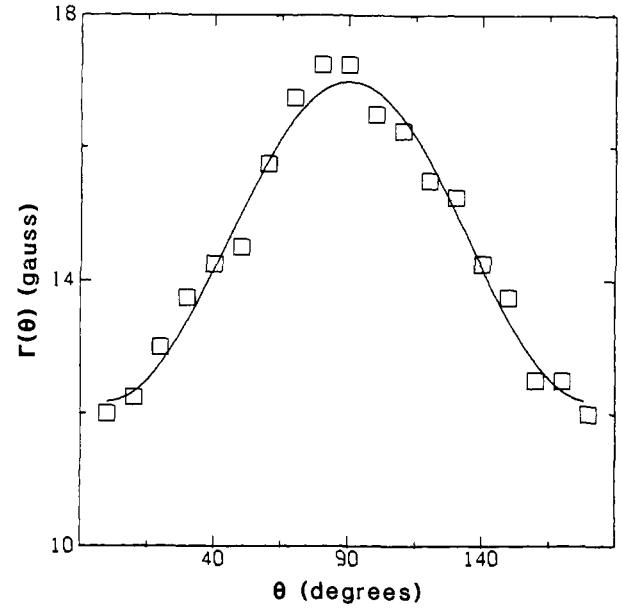

Figure 5. Angular dependence of the ESR line width at room temperature for $[Ni(tmp)]_2[PF_6]$. The solid line is the theoretical fit to eq 2.

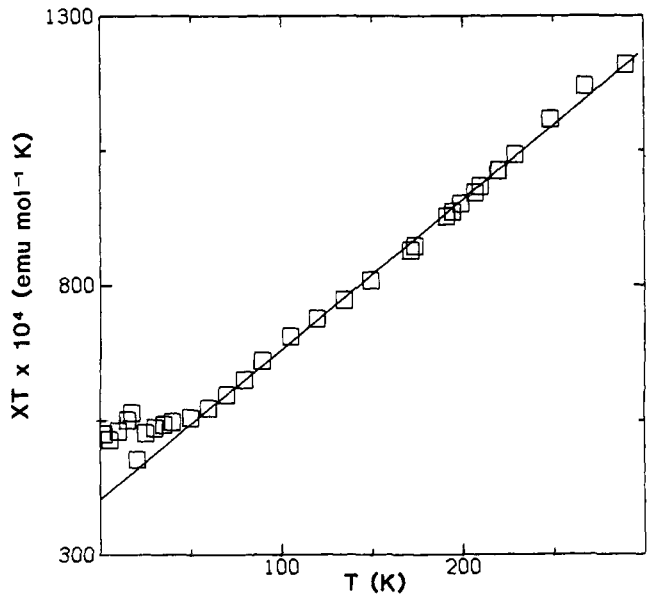

Figure 6. Temperature dependence of the product of temperature and susceptibility. The solid line is the theoretical fit to eq 3.

(17) For example see: (a) Wells, A. F. *Structural Inorganic Chemistry*; Clarendon Press: Oxford, 1984; p 851. (b) Cotton, F. A.; Matusz, M.; Rinaldo, P.; Feng, X. *J. Am. Chem. Soc.* **1988**, *110*, 1144–1154. (c) Gallois, B.; Gaultier, J.; Bechtel, F. *Mol. Cryst. Liq. Cryst.* **1987**, *148*, 279–293. (d) Tyagi, S.; Hathaway, B.; Kremer, S.; Stratemeier, H.; Reinen, D. *J. Chem. Soc., Dalton Trans.* **1984**, 2087–2091. (e) Carrtedo, G. A.; Howard, J. A. K.; Marsden, K.; Stone, F. G. A.; Woodward, P. *J. Chem. Soc., Dalton Trans.* **1984**, 1589–1595.

(18) McConnell, H. M.; Robertson, R. E. *J. Phys. Chem.* **1957**, *61*, 1018.

$$\Gamma(\theta) = \Gamma_0 + \Gamma_1 \sin^2 \theta \quad (2)$$

A least-squares fit of the experimental data (Figure 5) of Γ and θ to eq 2 yields constants of $\Gamma_0 = 12.2$ (4) G and $\Gamma_1 = 4.8$ (6) G. A phase-shifted form of eq 2 involving $\cos^2 \theta$ has been explained in terms of electron-spin dipole–dipole interactions that are exchange-narrowed.[6,19] The angular dependence of $\Gamma(\theta)$ here and of Ni(tmp)I[1] has yet to be explained. The line width decreases with temperature, becoming less than 1.0 G at 77 K. The anisotropy of Γ also decreases with temperature, and Γ is isotropic below 110 K.

Bulk Susceptibility Measurements. The measured room-temperature static susceptibility of a powdered sample of [Ni(tmp)]$_2$[PF$_6$] is $\chi = -1.30 \times 10^{-4}$ emu/mol. When corrected for temperature-independent diamagnetism ($\chi^d = -5.02 \times 10^{-4}$ emu/mol),[20] the paramagnetic susceptibility is $\chi^P = 3.72 \times 10^{-4}$ emu/mol. This value is comparable to that of 3.63×10^{-4} emu/mol measured for Ni(tmp)I. The temperature dependence of the quantity $\chi^P T$ is shown in Figure 6. The data indicate that χ^P follows the expression

$$\chi^P = C/T + K \quad (3)$$

where C is the Curie constant and K is a constant. The first term in eq 3 represents a Curie contribution to χ^P of noninteracting spins, while the second term corresponds to the Pauli paramagnetism of conduction electrons. A least-squares fit of the data ($T > 50$ K) yields $C = 0.0405$ (1) emu mol^{-1} K^{-1} and $K = 2.78$ (1) $\times 10^{-4}$ emu mol^{-1}. A fit of the data to the usual Curie–Weiss expression led to a zero value for the Weiss constant. These data sharply contrast with the ESR spin susceptibility of Ni(tmp)I, which remains constant from room temperature to 28 K and decreases sharply below that temperature.

An interpretation of the susceptibility of [Ni(tmp)]$_2$[PF$_6$] can be attempted by comparing the measured Curie constant to that expected for completely localized spins, C_0. From the relation

$$C_0 = S(S+1)\left[\frac{Ng^2\beta^2}{3k_B}\right] \quad (4)$$

where β is the Bohr magneton, k_B is Boltzmann's constant, S is the spin, g is the Lande factor, and N is the number of spin sites per mole, we can set $C_0 = C$ and determine a value for N, an effective number of noninteracting localized spins. The measured Curie constant of 0.0405 (1) emu mol^{-1} K^{-1} corresponds to 0.11 localized, noninteracting spins per Ni(tmp) molecule. This value is 22% of the maximum possible value because the degree of partial oxidation in the material is $+^1/_2$ and no more than 0.5 spin per macrocycle could be present. This value is strikingly large when compared to other metallomacrocyclic conductors and much too large to be accounted for by either lattice defect sites or paramagnetic metal impurities in the sample. In addition, it is not reasonable to suggest that the large Curie constant is associated with localized Ni(III) sites produced by partial oxidation of the metal ion, namely, a situation of "double mixed valency". If such a large proportion of Ni(III) sites were present, the ESR properties of this material would be very different from those observed. Thus, if the Ni(III) sites were not coupled to the carrier electrons they would give an independent signal in the ESR spectrum of the material in addition to the $g = 2$ signal of the carriers, but this is not observed. In contrast, if there were coupling between metal and carrier spins the g value of the ESR signal would be a weighted average that is shifted away from the free-electron value. Instead, we speculate that the value of the Curie constant reflects details of the band structure that arise from the approximately degenerate metalloporphyrin HOMOs.

Single-Crystal Electrical Conductivity. The room-temperature value of the electrical conductivity of [Ni(tmp)]$_2$[PF$_6$] single crystals measured along the needle (c) axis ranges from 10 to 150 Ω^{-1} cm^{-1}. This range is comparable to that observed for Ni(tmp)I (40–270 Ω^{-1} cm^{-1}),[1] lower than for the large-ring systems Ni(tbp)I (150–330 Ω^{-1} cm^{-1})[4] and Ni(pc)I (260–750 Ω^{-1} cm^{-1}),[6,21] but higher than for Ni(omtbp)I$_{1.08}$ (4–16 Ω^{-1} cm^{-1}).[5]

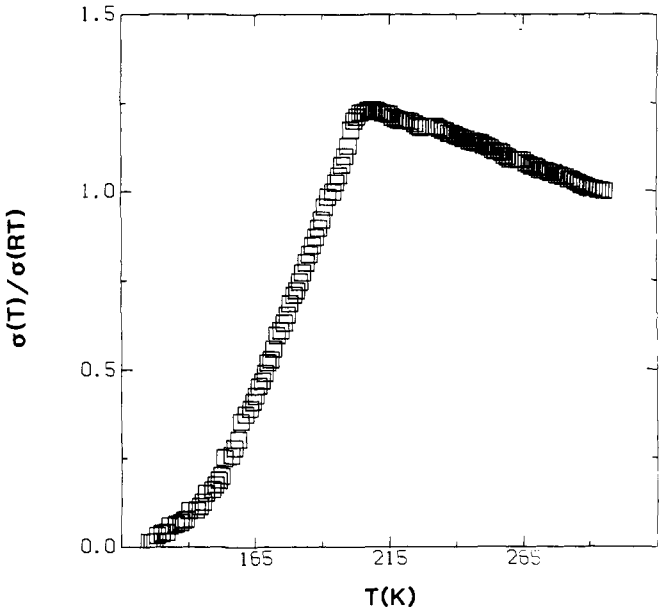

Figure 7. Temperature dependence of the conductivity for a single crystal of [Ni(tmp)]$_2$[PF$_6$] normalized to room temperature.

In one-electron band theory the conductivity can be related to $\bar{\lambda}_\parallel$, the mean free path of a carrier along the stacking direction (the average distance between scattering events), and to A, the cross-sectional area per conducting stack, by the relation

$$\sigma_\parallel = 2e^2\bar{\lambda}_\parallel/(hA) \quad (5)$$

where e is the electron charge and h is Planck's constant.[22] For [Ni(tmp)]$_2$[PF$_6$], $\bar{\lambda}_\parallel \sim 0.9$ Å, which is within the range found for Ni(tmp)I.[1] When expressed in units of intermolecular spacing along the stacking direction, $\bar{\lambda}_\parallel \sim {}^1/_4$. A value of $\bar{\lambda}_\parallel < 1$ is generally associated with a diffusion or hopping conductor. For comparison, Ni(pc)I has $\bar{\lambda}_\parallel > 1$, an indication that the conduction process is significantly wavelike.

Figure 7 presents the typical temperature dependence of the conductivity, normalized to the room-temperature value. At temperatures above 205 K, [Ni(tmp)]$_2$[PF$_6$] exhibits metallic conductivity ($d\sigma/dT < 0$) along the stacking axis. The conductivity reaches a maximum at 205 K, the value being about 1.25 times that measured at room temperature. Below 205 K, the conductivity decreases rapidly. Ni(tmp)I has an average room-temperature conductivity of 110 Ω^{-1} cm^{-1} and suffers a more gradual transition to activated behavior at roughly 115 K.

The transition from metallic to activated behavior in [Ni(tmp)]$_2$[PF$_6$] is reproducible and abrupt but does not result from a detectable structural change, as its crystal structures at 220 and 150 K are identical except for an expected slight decrease in lattice spacing because of thermal contraction. The transition could arise from the effects of potentials[23,24] created by the anion chains or crystal imperfections that tend to localize wave functions on the two-band conducting stack.[24]

Acknowledgment. We thank Dr. Kwangkyoung Liou for

(19) Soos, Z. G.; Huang, T. Z.; Valentine, J. S.; Hughes, R. C. *Phys. Rev. B: Solid State* **1973**, *8*, 993–1002.
(20) From Pascals constants, see: Drago, R. S. *Physical Methods in Chemistry*; W. B. Saunders: Philadelphia, 1977; p 413.
(21) Schramm, C. J.; Stojakovic, D. R.; Hoffman, B. M.; Marks, T. J. *Science (Washington, D.C.)* **1978**, *200*, 47–48.
(22) Berlinsky, A. J. *Contemp. Phys.* **1976**, *17*, 331–354.
(23) Borland, R. E. *Proc. Phys. Soc. London* **1961**, *78*, 926–931.
(24) (a) Bloch, A. N.; Weisman, R. B.; Varma, C. M. *Phys. Rev. Lett.* **1972**, *28*, 753–756. (b) Gruner, G.; Janossy, A.; Holczesr, K.; Mihaly, G. *Lect. Notes Phys.* **1979**, *96*, 246–254. (c) Epstein, A. J.; Conwell, E. M.; Miller, J. S. *Ann. N. Y. Acad. Sci.* **1978**, *313*, 183–209. (d) Epstein, A. J.; Miller, J. S. *Lect. Notes Phys.* **1979**, *96*, 265–272.

performing the EDAX experiments. This work was supported by the National Science Foundation through Grant DMR 88 18599 (B.M.H.) and through the Northwestern University Materials Research Center, Grant DMR 88 21571.

Supplementary Material Available: Table III listing anisotropi thermal parameters for $[Ni(tmp)]_2[PF_6]$ (1 page); Table IV listin calculated and observed structure amplitudes (8 pages). Orderin information is given on any current masthead page.

NMR Evidence for a Planar Arene Intermediate in the Electron-Transfer-Induced η^6 to η^4 Hapticity Change of a Rhodium Arene Complex†

Jon Merkert,‡ Roger M. Nielson,§ Michael J. Weaver,*,§ and William E. Geiger*,†

Contribution from the Departments of Chemistry, University of Vermont, Burlington, Vermont 05401, and Purdue University, West Lafayette, Indiana 47907.
Received December 22, 1988

Abstract: ^1H NMR spectra have been obtained for the Rh(II) complex $[(\eta^6\text{-}C_6Me_6)RhCp^*]^+$, $Cp^* = \eta^5\text{-}C_5Me_5$, at 200, 250, and 470 MHz. A single resonance was observed for the arene CH_3 protons between 298 and 183 K in CD_2Cl_2. The temperature dependence of the resonance was consistent with a doublet-state formulation of the Rh(II) complex. At 298 K, the CH_3 chemical shifts were 56 ppm for the arene substituents and 123 ppm for the cyclopentadienyl substituents. The magnetic equivalence of the arene methyl resonances is consistent with a planar arene structure in the complex. It is shown that a structural formulation including a highly fluxional bent arene is unlikely. The results demonstrate that when a metal complex undergoes a two-electron-transfer-induced change from η^6- to η^4-arene hapticity, the one-electron intermediate can retain the planar arene structure, even if this results in a 19-e^- metal.

Ligands with a variable hapticity may be important in the action of metal-based catalytic systems, since their electronic ambivalence allows low-energy associative and dissociative pathways.[1] The importance of this property has been identified in connection with both 16/18-electron diamagnetic systems[2] and with 17/19-electron radical systems.[3]

Muetterties and Bleeke pointed out that most catalyst precursors for arene hydrogenation have an accessible formal two-electron couple involving the d^6 and d^8 electronic configurations (eq 1).[4]

$$d^6\text{-}M^{n+2} + 2e^- \rightleftharpoons d^8\text{-}M^n \qquad (1)$$

They and others suggested[5-7] that the arene bends into a tetrahapto bonding mode to accommodate the two electrons gained in coordination of dihydrogen prior to transfer of 2H to the arene (Scheme I).

A key factor in this process was identified as the effect of the d^x electronic configuration on the energy of both the η^6 and η^4 arene complexes.[4] It is logical to address this problem by studies of model metal-arene complexes in which the $d^6 \rightleftharpoons d^8$ change occurs by transfer of two electrons rather than by transfer of H_2.[8-11]

Two redox systems have so far been reported that display the hexahapto/tetrahapto arene transformation upon receipt of two electrons by the metal, $[(\eta^n\text{-arene})Ru(\eta^6\text{-arene})]^{2+/0}$ (ref 10-12) and $[(\eta^n\text{-arene})MCp^*]^{2+/0}$, M = Rh or Ir, $Cp^* = \eta^5\text{-}C_5Me_5$.[8,9] Crucial to these studies is knowledge of the arene hapticity in the odd-electron intermediate. Arguments have been made, on the basis of the influence of arene substituents on the d^6/d^7 and d^7/d^8 formal potentials of a Rh(III)/Rh(II)/Rh(I) sequence[13a] and with utilization of kinetic data for electron exchange,[13b] that arene bending occurs in the second electron transfer. However, no direct spectroscopic or crystallographic evidence has been presented. We now report ^1H NMR data consistent with the assertion that the Rh(II) species in that series has a planar or nearly planar arene The d^7 intermediate is shown to prefer a 19-electron configuration

Scheme I

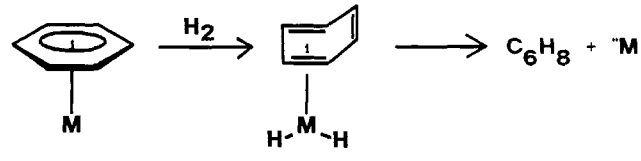

Scheme II

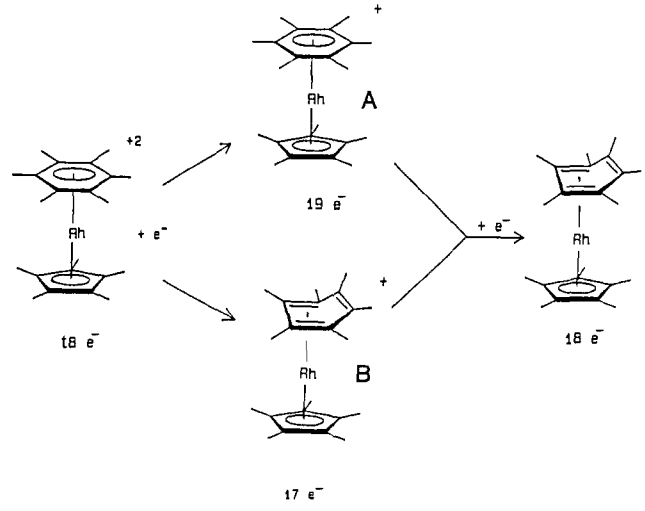

† This may be considered as part 19 of the series "Structural Consequence of Electron-Transfer Reactions". Part 18: Bowyer, W.; Merkert, J.; Geiger, W. E.; Rheingold, A. L. *Organometallics* **1989**, *8*, 191.

‡ University of Vermont.

§ Purdue University.

(1) Collman, J. P.; Hegedus, L. S.; Norton, J. R.; Finke, R. G. *Principles and Applications of Organotransitionmetal Chemistry*; University Science Books: Mill Valley, CA, 1978; p 524.
(2) Reference 1, Chapters 10, 11.
(3) Therien, M. J.; Trogler, W. C. *J. Am. Chem. Soc.* **1987**, *109*, 5127
(4) Muetterties, E. L.; Bleeke, J. R. *Acc. Chem. Res.* **1979**, *12*, 324
(5) Reference 1, pp 253-255.

0002-7863/89/1511-7084$01.50/0